Journal of Power Sources 193 (2009) 939–943

Contents lists available at ScienceDirect

Journal of Power Sources

journal homepage: www.elsevier.com/locate/jpowsour

Short communication

Synthesis and capacitive property of hierarchical hollow manganese oxide nanospheres with large specific surface area

Xiuhua Tang[a,b], Zong-huai Liu[a,b,*], Chengxiao Zhang[a,b], Zupei Yang[a,b], Zenglin Wang[a,b]

[a] Key Laboratory of Applied Surface and Colloid Chemistry (Shaanxi Normal University), Ministry of Education, Xi'an, 710062, PR China
[b] School of Chemistry and Materials Science, Shaanxi Normal University, Xi'an, 710062, PR China

ARTICLE INFO

Article history:
Received 9 October 2008
Received in revised form
29 December 2008
Accepted 21 April 2009
Available online 3 May 2009

Keywords:
Core-shell material
Mesoporous material
Layered manganese oxide
Capacitance

ABSTRACT

The hierarchical hollow manganese oxide nanospheres with both a large surface area and a layered structure have been successfully prepared by a templating-assisted hydrothermal process at 150 °C for 48 h. SiO_2 template spheres are dispersed in $KMnO_4$ solution, and then followed by hydrothermal treatment to forming silica/manganese oxide nanospheres with a core-shell structure. The core-shell nanospheres are etched in a NaOH solution (20 wt.%), so that the SiO_2 core is removed, and the hierarchical hollow manganese oxide nanospheres are obtained. The as-synthesized hierarchical hollow manganese oxide nanospheres present a birnessite-type manganese oxide phase with a chemical composition of $Na_{0.38}MnO_{2.14}\cdot 13H_2O$, and a specific surface area of 253 $m^2\,g^{-1}$. The prepared materials exhibit an ideal capacitive behavior and good cycling stability in a neutral electrolyte system and the initial capacitance value is 299 $F\,g^{-1}$. Some preparation conditions including the hydrothermal temperature, dwell time and concentration of template have been also investigated.

1. Introduction

Electrochemical supercapacitors based on manganese oxides as active electrode materials are currently attracting a lot of interest due to the relatively low cost, low toxicity, excellent electrochemical performance, environmentally friendly character in compare with the ruthenium oxides or other transition metal oxides [1–3]. Up to now, many manganese oxides with various structures and morphologies have been fabricated via electrochemical and chemical routes, and their electrochemical properties have been investigated. The investigated materials mainly focus on the amorphous or poorly crystallized manganese oxides, manganese oxide thin films [4–6]. The research results indicate that manganese dioxide powers have shown an average specific capacitance of 160 $F\,g^{-1}$, while the manganese dioxide thin films have a capacitance in the range between 100 $F\,g^{-1}$ and 400 $F\,g^{-1}$ due to high utilization of material [7–9], which are far from the theoretical specific capacitance of ~1000 $F\,g^{-1}$. Therefore, manganese oxides with high specific capacitance, good cyclic stability and low fabrication cost are expected.

In general, the specific capacitance of the cathode materials is related to its specific surface area, the electrical conductivity in the solid phase and ionic transport within the pores because the larger specific surface area and good ionic transport can lead to a higher current density and facilitate the fast transport of electrolyte with metal ions [10]. In this regard, a layered structure consisting of bicontinuous networks of solid and pore on the nanometer scale is an attractive candidate for application as active electrode material, and especially in the mesoporous birnessite-type manganese oxide with large specific surface area. Till now, although birnessite-type manganese oxides with different morphologies such as nanobelt [11,12], flower-like microsphere [13], nanobundles [14], flower-like nanowhisker [15], and so on have been prepared, the obtained materials have less specific surface area (in the range between 20 $m^2\,g^{-1}$ and 150 $m^2\,g^{-1}$) [16], which limits their applications as active materials for supercapacitor. Thus research on the preparation method to create nanostructure active materials with large specific surface area is of great significance.

Herein hierarchical hollow manganese oxide nanospheres with both a large surface area and a layered structure were successfully prepared by a templating-assisted hydrothermal process at 150 °C for 48 h. As shown in Fig. 1, the synthesis is preformed by a two-step process. SiO_2 employed spheres was first dispersed in $KMnO_4$ solution and then followed by a hydrothermal treatment to form a silica/manganese oxide core-shell nanosphere. The core-shell nanosphere was etched in a NaOH solution (20 wt.%), so that the SiO_2 core was removed, and hierarchical hollow manganese oxide nanospheres with a large specific surface area of 253 $m^2\,g^{-1}$ were prepared. The as-prepared hierarchical hollow manganese oxide nanospheres exhibited an ideal initial capacitive behavior of 299 $F\,g^{-1}$ and good cycling stability in a neutral electrolyte system.

* Corresponding author. Tel.: +86 29 85308442; fax: +86 29 85307774.
E-mail address: zhliu@snnu.edu.cn (Z.-h. Liu).

0378-7753/$ – see front matter © 2009 Elsevier B.V. All rights reserved.
doi:10.1016/j.jpowsour.2009.04.037

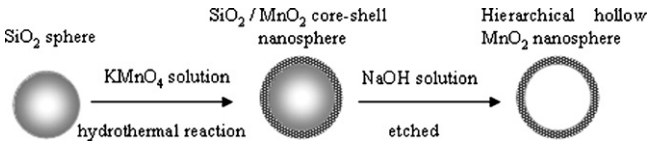

Fig. 1. Sythesis process of hierarchhical hollow manganese oxide nanosphere.

2. Experimental

2.1. Materials synthesis

The template, SiO_2 sphere, was prepared with ultrasonic method reported in a literature [17]. Under ultrasonic condition (240 W, 40 kHz), tetraethoxysilane (3 mL) was dropped into a mixture of absolute ethanol (50 mL) and ammonia (6 mL) with a rate of eight drops per minute. During the ultrasonic process, the temperature was maintained at 40 °C throughout. The obtained SiO_2 suspension was centrifuged, rinsed with distilled water, and redispersed in H_2O (12 mL) to finally form SiO_2 white suspension.

$KMnO_4$ (0.73 g) was added to the SiO_2 white suspension and treated by ultrasonic treatment for 30 min, a purple suspension was obtained. The obtained purple suspension was then transferred to a Teflon-lined autoclave and followed by treating at 150 °C for 48 h; the brown intermediate sediment with a silica/manganese oxide core-shell structure was obtained, which was abbreviated as SMS. The brown intermediate sediment with core-shell structure was etched in a NaOH solution (20 wt.%), and then the SiO_2 core was dissolved. After the removal of SiO_2 core with NaOH, the final products, the hierarchical hollow manganese oxide nanospheres were obtained after centrifugation, and washed for several times with ultrapure water, which were abbreviated as HMS.

2.2. Characterizations

X-ray diffraction pattern (XRD) measurements were carried out with a Rigaku D/Max2550VB + /PC instrument using graphite-monochromated Ni-filtered Cu Kα radiation. A Quanta 200 environmental scanning electron microscopy was used to observe the morphologies of the precursors, the intermediate sediments and final products. For TEM observation, the samples were redispersed in ethanol by ultrasonic treatment and dropped on carbon–copper grids. TEM images were collected by using a JEOL-JEM-3010 microscope working at 120 kV. A Fourier Transform Infrared Spectrometer EQUINX55 was used to obtain the infrared spectra of the samples by the KBr method. A Beckman coulter-type nitrogen adsorption–desorption apparatus was used to investigate the pore property degassing for 4 h below 10^{-3} mmHg. Mn and Na contents were determined by atomic absorption spectrometry after samples were dissolved in a mixed solution of HCl (1.0 mol L^{-1}) and H_2O_2 (28%) (v/v = 5:1). The content of H_2O was determined by weight loss under 120 °C in thermogravimetric analysis (TGA).

2.3. Electrochemical measurement

Electrodes were prepared by mixing MnO_2 power (75 wt.%) as active material with acetylene black (20 wt.%), and polyvinylidene fluoride (5 wt.%). The two former constituents were first mixed together to obtain a homogeneous black power. The polyvinylidene fluoride solution (0.02 g mL^{-1}, in *N*-methyl-ketopyrrolidine) was then added. This resulted in a rubber-like paste, which was brush-coated onto a Ni mesh. The mesh was dried at 110 °C in air for 2 h for the removal of the solvent. After drying, the coated mesh was uniaxially pressed to more completely adhere the electrode material with the current collector.

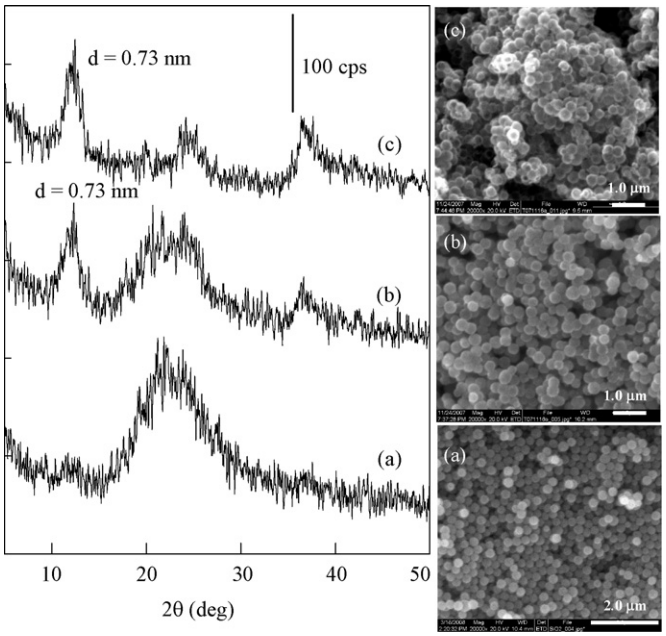

Fig. 2. XRD patterns (left) and SEM images (right): (a) SiO_2 spheres, (b) SMS, and (c) HMS.

A CHI 600 electrochemical workstation (Chenhua Instrument Co., Shanghai, China) was used for electrochemical measurements. A beaker type electrochemical cell equipped with a MnO_2 based working electrode, a Pt-foil (2 cm^2) as the counter electrode and saturated calomel electrode (SCE) as the reference electrode. CV curves were done between −0.2 V and 0.8 V in a Na_2SO_4 electrolyte (1 mol L^{-1}) at a sweep rate of 5 mV s^{-1}. The average specific capacitance was evaluated from the area of the charge and discharge curves of the CV plot [18].

3. Results and discussion

The prepared templating SiO_2 shows a non-crystalline character and regular monodisperse sphere morphology, the size of the sphere ranges from 200 to 350 nm (Fig. 2a). By hydrothermally treating $KMnO_4$ purple suspension with SiO_2 dispersed at 150 °C for 24 h, brown intermediate sediment with silica/manganese oxide core-shell structure (SMS) was obtained. In general, manganese oxides with layered structure contain a set of basal reflections with *d* values that correspond to a minimum periodicity along *c* equal to 0.72 nm, which is the basic characteristic of layered structure. The XRD pattern of sample SMS shows a reflection characteristic of a typical birnessite-type manganese oxide, the diffraction peaks at about 12.5°, 25° and 37.5° can be observed, corresponding to a basal spacing of 0.73 nm (Fig. 2b). These peaks are almost in accord with characteristic diffraction peaks of birnessite-type manganese oxide crystal (JCPDS 23-1046), while the particle morphology hardly changes. Sample SMS was etched in NaOH solution (20 wt.%), the SiO_2 core was dissolved and the hierarchical hollow manganese oxide nanospheres (HMS) were obtained. The broad and low diffraction peaks suggest that the sphere particles of the sample HMS are small in size. In comparison with the particle morphology of the sample SMS, sample HMS shows identical morphology and particle size distribution (Fig. 2c).

Transmission electron microscopy (TEM) observations reveal that the intermediate sample SMS shows monodispersed sphere morphology, and the hierarchical spherical morphology can be clearly observed in a larger-magnification image (Fig. 3b). Zeng and co-workers reported ZnS homogeneous core-shells can be

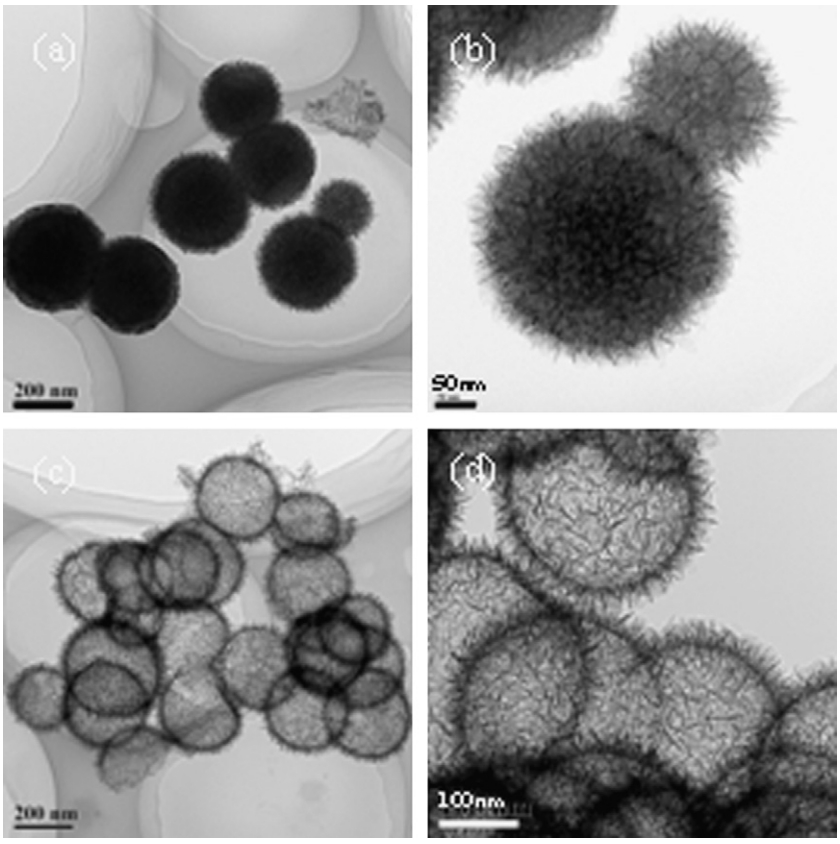

Fig. 3. TEM images of SMS (a and b) and HMS (c and d) at different magnifications.

synthesized via Ostwald ripening in a one-pot synthesis [19]. In the present experiment, the formation of silica/manganese oxide shell/core intermediate structure is also explained according to a Ostwald ripening process. The manganese oxide shell starts from the surface nucleation on the SiO_2 templating sphere. Due to the Ostwald ripening, the manganese oxide crystallites on the SiO_2 surface become larger ones on attracting the smaller crystallites underneath, and final manganese oxide nanocrystals with extended and curled thin pieces aggregating on the SiO_2 surface. After SiO_2 template core was removed by NaOH solution, the hierarchical hollow manganese oxide nanospheres with hollow inner cavity and thin outer shell were obtained. Further observation for the magnification TEM image shows that the wall thickness of the nanosphere is ca. 35 nm (Fig. 3d) and the sphere surface is rough. These results indicate that the obtained hierarchical hollow manganese oxide nanospheres are small in size and a large hollow inner cavity is existed.

In contrast with the FT-IR spectrum of the intermediate sample SMS, a characteristic O–Si–O absorption bands around 1109 cm^{-1} and 807 cm^{-1} were completely disappeared in sample HMS after sample SMS was soaked in NaOH solution, indicating that the template SiO_2 sphere was removed from the core-shell structure (Fig. 4) [20]. In addition, the Mn–O stretching vibration band around 479 cm^{-1} shifted to a higher frequency (511 cm^{-1}) due to the removal of the templating SiO_2.

The effects of the hydrothermal temperatures on the morphology and crystalline of the intermediate sample SMS and the final product HMS shows that a relatively good hierarchical hollow manganese oxide nanospheres are obtained at 150 °C (Figure S1). The obtained samples at different hydrothermal temperatures have a typical XRD pattern of birnessite-type manganese oxide (Figure S2). Above or below this temperature, the final products show irregular agglomeration sphere morphologies. At low temperatures, less manganese oxide nanocrystals are aggregated on the surface of templating SiO_2 spheres and a thin shell structure is formed. Because the shells are thin enough, they collapse and agglomerate to form irregular sphere morphologies when the SiO_2 template is removed. On the other hand, $KMnO_4$ quickly decomposes and forms a lot of manganese oxide nanocrystals which aggregate irregularly on the surface of SiO_2 templating spheres under a higher temperature condition.

Time-dependent experiments were carried out by hydrothermally treating the suspension of $KMnO_4$ and SiO_2 spheres at 150 °C for different reaction times. The obtained intermediate samples and final products show an aggregated morphology with prolonging the hydrothermal dwell time (Figure S3). The relatively high hydrother-

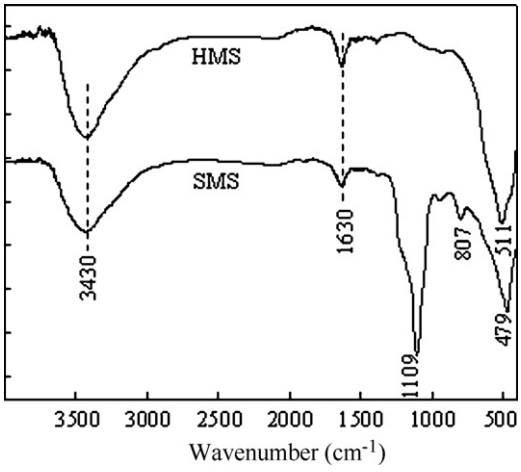

Fig. 4. FT-IR spectra of samples SMS and HMS.

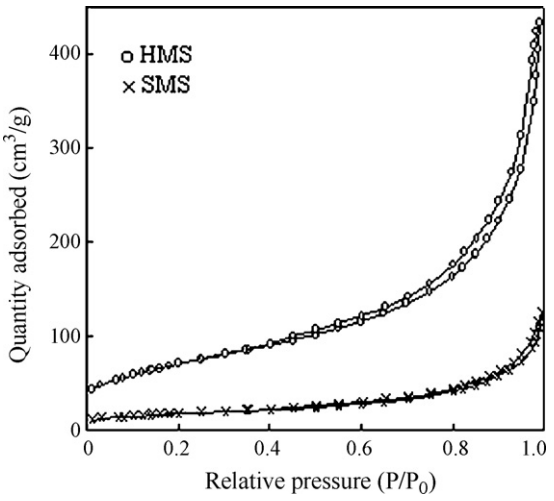

Fig. 5. N_2 adsorption–desorption isotherms for samples SMS and HMS.

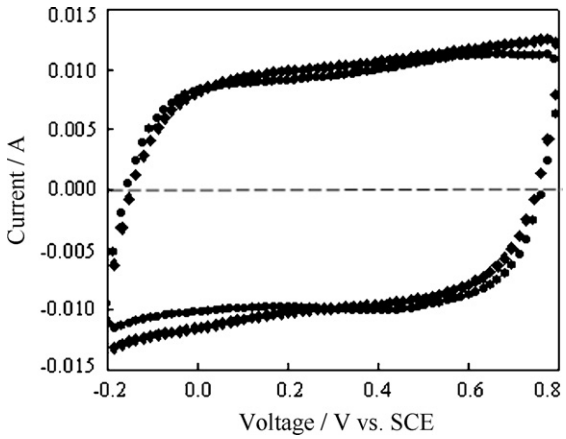

Fig. 6. The 1st (♦) and 1000th (●) cyclic voltammogram cycle curves of sample HMS at a scan rate of 5 mV s^{-1} in 1 M Na_2SO_4 solution.

mal temperature destroys the surface of SiO_2 sphere in some extent, and the longer time the hydrothermal treatment dwelled, the more seriously the surface of SiO_2 sphere were destroyed. In addition, the morphology effect of template SiO_2 amount on the final products shows cluster-like morphology product is obtained when no SiO_2 template is used, which are agglomerated by small birnessite-type manganese oxide particles (Figure S4). With the increase of SiO_2 template amounts, the intermediate products with both sphere and cluster morphologies are obtained, and a final product with homogenous spherical morphology is formed when the amount of SiO_2 template spheres increases to 1.2 mol L^{-1}.

N_2 adsorption–desorption isotherms of sample HMS in comparison with sample SMS are shown in Fig. 5. Sample SMS is apparently non-porous, having a Brunauer–Emmett–Teller (BET) surface area of 59 m^2 g^{-1}. In contrast, the isotherm feature of sample HMS clearly indicates the presence of mesopores in this sample, classified as type IV as defined by the International Union of Pure and Applied Chemistry (IUPAC) [21]. A hysteresis loop between the adsorption and desorption branches can be considered as type H3, indicative of slit-like pores. It should be noted that pillared manganese oxides obtained through the conventional intercalation are mostly microporous [22-24]. The sample HMS with hierarchical hollow morphology shows a much higher BET surface area of 253 m^2 g^{-1} and larger N_2 adsorption volume. The BET surface area is obviously larger than that reported by Wei and co-workers [15], in which nanostructured MnO_2 with mixed nanorods and nanostructured surface with a distinct plate-like morphology was obtained and its BET surface area was of 132 m^2 g^{-1}. The specific capacitance was 168 F g^{-1}. A *t*-plot analysis confirms the predominant presence of mesopores in sample HMS. The mesoporous surface area is about 218 m^2 g^{-1}, and contributed to about 86% of the total specific surface area. These results clearly indicate that the formation of the hierarchical hollow in sample HMS drastically enhances the mesoporosity as well as the specific surface area. This mesoporous nature may be principally elucidated by the hollow inner cavity and thin outer shell of hierarchical hollow manganese oxide nanospheres.

There have been only a few reports on mesoporous manganese oxides with birnessite-type structure. One has a pore-solid architecture of nanoscale MnO_2 with the birnessite structure, which can be controlled based on the methods employed to render the dry gel [25]. Chen et al. reported the preparation of mesoporous layered manganese oxide nanospheres with honeycomb and hollow morphologies at room temperature by varying the molar ratio of $KMnO_4$ and oleic acid [26]. Wang et al. synthesized a new mesoporous manganese oxide with a layered structure via restacking colloid MnO_2 nanosheets with Al_{13} Keggin ions, which has a well-developed structural mesoporosity with a remarkably high specific surface area of 204 m^2 g^{-1} [27]. In the present work, mesoporous hierarchical hollow manganese oxide nanospheres with a layered structure is prepared, and the large specific surface area may be principally carried out by the hollow inner cavity and thin outer shell of hierarchical hollow manganese oxide nanospheres, which is different from the above-mentioned architectures.

Manganese oxides with various valence states and crystalline structure are currently investigated for electrochemical electronic, catalytic and other applications. Extensive studies have shown that manganese oxides are promising electrode materials for electrochemical supercapacitors. Cyclic voltammetry is an important tool to investigate the capacitive behavior of materials. Fig. 6 shows the 1st and the 1000th cyclic voltammetry curves for the hierarchical hollow manganese oxide spheres electrode prepared. The CV curves obtained in a Na_2SO_4 (1 mol L^{-1}) solution at a sweep rate of 5 mV s^{-1} show relatively rectangular mirror images with respect to the zero-current line. The rectangular mirror images indicate the capacitive behavior for the obtained materials. It is clear from Fig. 6 that there are no redox peaks in the range between −0.2 V and 0.8 V, indicating the hierarchical hollow manganese oxide sphere electrode prepared by the present method behaves as an ideal capacitor within the window of −0.2–0.8 V. The specific capacitance values calculated from the cyclic voltammetry curves are found to be 299 F g^{-1} and 291 F g^{-1}, respectively. The variation of the specific capacitance as a function of cycle number shows that the specific capacitance slightly decreases with increasing the cycle number. After 1000 cycles of the operation, the electrode can maintain 97.6% of the initial value, indicating the good cycling stability of the hollow manganese oxide sphere electrode materials (Fig. 7). TEM image shows that the hollow structure of the obtained material is mainly maintained after 1000 cycles, and some destruction of the hierarchical spherical morphology is observed in some scale (Figure S5).

On the other hand, the electrochemical properties of MnO_2 non-hollow nanoparticles obtained without the silica template the MnO_2 show an obvious difference in comparison with the hollow manganese oxide nanospheres. The 1st and the 200th cyclic voltammetry curves show that although the CV curves close to rectangular mirror images, a lower specific capacitance of 163 F g^{-1} is calculated from 1st cyclic voltammetry curve. After 200 cycles, the specific capacitance decreases to 106 F g^{-1}, 65% of the initial value, indicating the cluster-like product has not good cycling stability (Figure S6). Therefore, the hollow manganese oxide nanospheres show a good capacitance property.

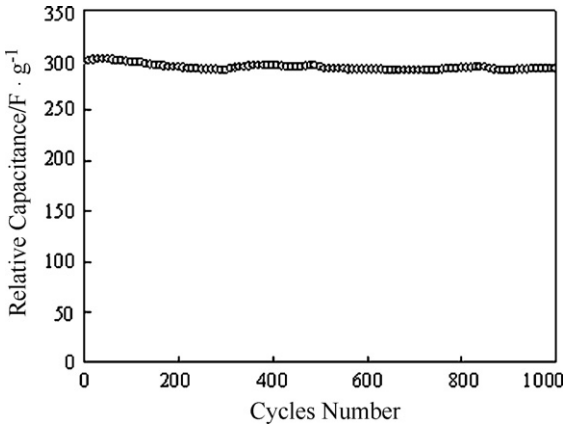

Fig. 7. Variation of the specific capacitance with respect to cycle number. The potential cycling was performed in 1.0 M Na_2SO_4 within a potential window ranging from −0.2 V to +0.8 V vs Hg/Hg_2SO_4 at a sweep rate of 5 mV s^{-1}.

Until now, two mechanisms have been proposed to explain the MnO_2 charge storage behavior. The first mechanism is based on the concept of intercalation of H^+ or alkali metal cations such as Na^+ ions in the electrode during reduction and deintercalation upon oxidation.

$$MnO_2 + A + e^- \leftrightarrow MnOOA$$

And the secondary one is based on the surface adsorption of electrolyte cations.

$$(MnO_2)_{surface} + A + e^- \leftrightarrow (MnO_2{}^-A)_{surface}$$

In the present study, we think that the redox process is mainly governed by the intercalation and deintercalation of Na^+ ions from the electrolyte into the mesoporous hollow manganese oxide spheres, similar to the work reported by Toupin et al. [28].

In summary, the hierarchical hollow manganese oxide nanospheres with a large surface area were successfully prepared by a templating-assisted hydrothermal process at 150 °C for 48 h. It created a novel route to prepare mesoporous birnessite-type manganese oxides with a large surface area. The experimental optimized conditions of the hierarchical hollow manganese oxide nanospheres were obtained. The as-prepared hollow manganese oxide nanosphere not only had a large area of 253 $m^2\,g^{-1}$, but also showed an ideal capacitive behavior and good cycling stability in a neutral electrolyte system. The ideal capacitive behavior with a specific capacitance of 299 F g^{-1} was found and the specific capacitance only decreased by 2.4% after 1000 cycles.

Acknowledgment

We thank National High Technology Research and Development Program of China (2007AA03Z248) and Key Project of the Minister of Education, China for Researching on Science and Technology (106148) for financial support this research.

Appendix A. Supplementary data

Supplementary data associated with this article can be found, in the online version, at doi:10.1016/j.jpowsour.2009.04.037.

References

[1] X.Y. Wang, W.G. Huang, P.J. Sebastian, S. Gamboa, J. Power Sources 140 (2005) 211–215.
[2] M. Toupin, T. Brousse, D. Bélanger, Chem. Mater. 14 (2002) 3946–3952.
[3] L. Athouël, F. Moser, R. Dugas, O. Crosnier, D. Bélanger, T. Brousse, J. Phys. Chem. C 112 (2008) 7270–7277.
[4] C.J. Xu, B.H. Li, H.D. Du, F.Y. Kang, Y.Q. Zeng, J. Power Sources 180 (2008) 664–670.
[5] S.L. Chou, F.Y. Cheng, J. Chen, J. Power Sources 162 (2006) 727–734.
[6] B. Dong, T. Xue, C.L. Xu, H.L. Li, Microporous Mesoporous Mater. 112 (2008) 627–631.
[7] C.K. Lin, K.-H. Chuang, C.-Y. Lin, C.Y. Tsay, C.-Y. Chen, Surf. Coat. Technol. 202 (2007) 1272–1276.
[8] M. Nakayama, A. Tanaka, Y. Sato, T. Tonosaki, K. Ogura, Langmuir 21 (2005) 5907–5913.
[9] K.-W. Nam, M.G. Kim, K.-B. Kim, J. Phys. Chem. C 111 (2007) 749–758.
[10] J.Y. Luo, L. Cheng, Y.Y. Xia, Electrochem. Commun. 9 (2007) 1404–1409.
[11] R.Z. Ma, Y. Bando, L.Q. Zhang, T. Sasaki, Adv. Mater. 16 (2004) 918–922.
[12] Z.P. Liu, R.Z. Ma, Y. Ebina, K. Takada, T. Sasaki, Chem. Mater. 19 (2007) 6504–6512.
[13] L.C. Zhang, L.P. Kang, H. Lv, Z.K. Su, K. Ooi, Z.-H. Liu, J. Mater. Res. 23 (2008) 780–789.
[14] J.C. Ge, L.H. Zhuo, F. Yang, B. Tang, L.Z. Wu, C. Tung, J. Phys. Chem. B 110 (2006) 17854–17859.
[15] V. Subramanian, H.W. Zhu, B.Q. Wei, J. Power Sources 159 (2006) 361–364.
[16] V. Subramanian, H.W. Zhu, R. Vajtai, P.M. Ajayan, B.Q. Wei, J. Phys. Chem. B 109 (2005) 20207–20214.
[17] V.G. Pol, D.N. Srivastava, O. Palchik, V. Palchik, M.A. Slifkin, A.M. Weiss, A. Gedanken, Langmuir 18 (2002) 3352–3357.
[18] C.Z. Yuan, B. Gao, X.G. Zhang, J. Power Sources 173 (2007) 606–612.
[19] B. Liu, H.C. Zeng, J. Am. Chem. Soc. 126 (2004) 16744–16746.
[20] H. Kim, J. Cho, Chem. Mater. 20 (2008) 1679–1681.
[21] M. Kruk, M. Jaroniec, Chem. Mater. 13 (2001) 3169–3183.
[22] Z.-H. Liu, K. Ooi, H. Kanoh, W. Tang, X. Yang, T. Tomida, Chem. Mater. 13 (2001) 473–478.
[23] Z.-H. Liu, X.H. Tang, C.X. Zhang, Q. Zhou, Chem. Lett. 34 (2005) 1312–1313.
[24] Y. Ma, S.L. Suib, T. Ressler, J. Wong, M. Lovallo, M. Tsapatsis, Chem. Mater. 11 (1999) 3545–3554.
[25] J.W. Long, R.M. Stroud, D.R. Rolison, J. Non-Cryst. Solids 285 (2001) 288–294.
[26] H. Chen, J. He, C. Zhang, H. He, J. Phys. Chem. C 111 (2007) 18033–18038.
[27] L.Z. Wang, Y. Ebina, K. Takada, K. Kurashima, T. Sasaki, Adv. Mater. 16 (2004) 1412–1416.
[28] M. Toupin, T. Brousse, D. Bélanger, Chem. Mater. 16 (2004) 3184–3190.